

Coexistence of Ferroelectric Phases and Phonon Dynamics in Relaxor Ferroelectric $\text{Na}_{0.5}\text{Bi}_{0.5}\text{TiO}_3$ Based Single Crystals

Jiajun Zhu,[‡] Jinzhong Zhang,[‡] Kai Jiang,[‡] Haiwu Zhang,[§] Zhigao Hu,^{‡,†} Haosu Luo,[§] and Junhao Chu[‡]

[‡]Department of Electronic Engineering, East China Normal University, Shanghai 200241, China

[§]Key Laboratory of Inorganic Functional Material and Device, Shanghai Institute of Ceramics, Chinese Academy of Sciences, Shanghai 201800, China

A combination of polarized Raman technique, infrared reflectance spectra, and first-principles density-functional theoretical calculations were used to investigate structure transformation and lattice vibrations of $\text{Na}_{0.5}\text{Bi}_{0.5}\text{TiO}_3$, $\text{Na}_{0.5}\text{Bi}_{0.5}\text{TiO}_3$ -5% BaTiO_3 , and $\text{Na}_{0.5}\text{Bi}_{0.5}\text{TiO}_3$ -8% $\text{K}_{0.5}\text{Bi}_{0.5}\text{TiO}_3$ single crystals. It was found that $\text{Na}_{0.5}\text{Bi}_{0.5}\text{TiO}_3$ is of a two-phase mixture with rhombohedral and monoclinic structures at room temperature. Correspondingly, three Raman-active phonon modes located at 395, 790, and 868 cm^{-1} , which were previously assumed as A_1 modes of rhombohedral phase have been reassigned as A' , A'' , and A' modes of monoclinic phase in the present work. In particular, a strong low-frequency A'' mode at 49 cm^{-1} was found and its temperature dependence was revealed. Two deviations from linearity for the abrupt frequency variation in the A'' mode and Ti–O bond have been detected at temperatures of ferroelectric to antiferroelectric phase transition $T_{\text{F-AF}}$ and dielectric maximum temperature T_{max} . The appearance of Na–O vibrations at 150 cm^{-1} was found below T_{max} , indicating the existence of nanosized Na^+TiO_3 clusters. The observed Raman and infrared active modes belonging to distinct irreducible representations are in good agreement with group-theory predictions, which suggests $9A_1+9E$ and $36A''+24A'$ modes for the rhombohedral and monoclinic phases of $\text{Na}_{0.5}\text{Bi}_{0.5}\text{TiO}_3$, respectively.

Keywords: Raman spectroscopy; relaxor ferroelectrics; phase transitions

I. Introduction

PEROVSKITE ABO_3 ferroelectrics are extraordinarily attractive from fundamental and technological point of views due to excellent electrical, magnetic, structural, and optical properties.^{1–4} They undergo structural phase transitions with decreasing temperature, leading to lower the global symmetry of the crystal. According to different sorts of instability, these distortions are classified as Jahn–Teller (JT), ferroelectric (FE), and antiferrodistortive (AFD). Both JT and FE distortions are related to internal deformations of the BO_6 octahedra, while AFD ones are associated with coordinated rotations of nearly rigorous BO_6 octahedra. Comprehending the origin of the distortions and interaction is important to utilize their excellent properties. Ferroelectrics are sensitive to chemistry, defects, electrical boundary conditions, temperature, and pressure caused by a delicate balance between long-range Coulomb forces favoring the ferroelectric state

and short-range repulsions preferring the nonpolar cubic phase.¹ For FE distortions, the hybridization of empty d or s orbitals is localized on A or B cations, respectively, and that of occupied p orbitals are localized on the O^{2-} anions.

Relaxors $(1-x)\text{Na}_{0.5}\text{Bi}_{0.5}\text{TiO}_3$ - $x\text{BaTiO}_3$ (NBBT), $\text{PbZr}_{1-x}\text{Ti}_x\text{O}_3$ (PZT) and $\text{Pb}(\text{Mg}_{1/3}\text{Nb}_{2/3})\text{O}_3$ - PbTiO_3 (PMN-PT) show morphotropic phase boundaries (MPB) in the composition phase diagrams, where the crystal structure changes abruptly and the piezoelectric response is maximal due to symmetry-allowed polarization rotation.^{2,5} Although lead-based ferroelectrics, such as PZT and PMN-PT, are well studied and widely used from medical ultrasound and sonar to energy harvesting, they are environmentally undesirable due to the toxicity of lead. The lone-pair cation Bi^{3+} is regarded as a natural replacement candidate of Pb^{2+} owing to the electronic similarities. Both of them have large ionic radius, large number of electrons and a lone electron pair, which contribute to the distortion of the structure and piezoelectric response.⁶ Therefore, a growing interest in Bi-containing perovskites has been triggered by the necessity to replace lead-based ferroelectrics.

However, most bismuth perovskites, such as BiCrO_3 and BiMnO_3 , require high-pressure synthesis due to the small size of the Bi^{3+} ion. Such difficulty is a hindering factor for wide investigations and applications. Therefore, studies mainly focus on merely two stable materials: the multiferroic bismuth ferrite BiFeO_3 with simultaneous ferroelectric and magnetic ordering as well as $\text{Na}_{0.5}\text{Bi}_{0.5}\text{TiO}_3$ (NBT).^{7–9} On the other hand, NBT belongs to an A-site-substituted distorted perovskite compound, unlike the common B-site-substituted counterparts, such as PMN-PT. The electrical properties of NBT can be improved by the formation of solid solution with BaTiO_3 (BT) or $\text{Bi}_{0.5}\text{K}_{0.5}\text{TiO}_3$ (KBT),^{10,11} which exhibits excellent electromechanical properties around the MPB region.

The crystal structure of NBT is rhombohedral $R3c$ and that of KBT is tetragonal $P4bm$ at room temperature.¹² Coexistence of both phases can be found in the MPB region. According to the reported phase diagram of NBBT crystals, they crystallize in the rhombohedral $R3c$ ferroelectric phase, the tetragonal $P4bm$ relaxor ferroelectric phase, and the tetragonal $P4mm$ ferroelectric phase for $x \leq 6\%$, $5\% \leq x \leq 11\%$, and $x \geq 10\%$, respectively.¹³ Thus, a coexistence of rhombohedral $R3c$ and tetragonal $P4bm$ symmetries appears around $5\% \leq x \leq 6\%$. However, structure of NBT is far from resolved. Growing experimental evidences about the departure from pure rhombohedral symmetry have been recently reported. Gorfman and Thomas found that the splitting of Bragg peaks observed in the high-resolution reciprocal-space maps, which suggests that the average structure of NBT has lower than rhombohedral symmetry.¹⁴ Later on, Aksel et al. pointed out that their high-resolution powder X-ray diffraction patterns reveal peak splitting in the room-temperature phase that evidence the true structure as

J.L. Jones—contributing editor

monoclinic.¹⁵ Moreover, their Raman spectra are consistent with a previous assignment of a rhombohedral structure. They argued that their Raman result does not exclude the presence of a monoclinic phase on average because Raman spectroscopy is sensitive to the short-range crystalline order, which at room temperature is dominated by the B-site polarization along the rhombohedral [111] axis.¹⁶ Very recently, Rao et al. reported a subtle phase boundary at $x = 0.03$ for NBBT systems, which revealed that for $x < 0.03$ it is rhombohedral + monoclinic structural state.¹⁷ Moreover, their previous high-resolution synchrotron X-ray diffraction study revealed that NBT is best described in terms of a rhombohedral + monoclinic phase coexistence model.¹⁸ High-resolution synchrotron X-ray powder diffraction analysis demonstrates that the fraction of two coexisting ferroelectric rhombohedral and monoclinic phases is highly susceptible to thermal, mechanical, and electrical stimuli at room temperature.^{14–19} The subtle monoclinic phase gives a new dimension into understanding temperature dependence of the phase transitions in NBT.

Noncontact and nondestructive Raman spectroscopy represents an advantageous tool in electronics, which suits the technological needs for locally and quantitatively assessing crystal structures, domain textures, crystallographic misalignments, and residual stresses in piezoelectric materials. Thus, Raman spectroscopy has been widely used as a powerful probe to establish phase diagrams and to clarify complex phase transition of piezoelectric materials.^{20,21} Raman spectroscopy is an appropriate technique for the investigation of ionic configurations on length scales shorter than 10 nm, which is easily missed in X-ray diffraction. Due to different selection rules, infrared (IR) and Raman techniques offer the complementary results. Raman and theoretical studies on NBT are limited to its rhombohedral phase,^{22,23} which cannot fully explain the recent X-ray powder diffraction,^{14–18} neutron powder diffraction,¹⁹ and transmission electron microscopy evidences of monoclinic phase in pure NBT.²⁴ In this work, phonon modes of NBT are assigned according to temperature-dependent Raman scattering and IR spectra as well as from first-principles calculations with consideration of both rhombohedral and monoclinic phases. Several new vibrational modes, which are related to A' and A'' from monoclinic phase, are reported in the present work.

II. Experimental Procedure

NBT, $\text{Na}_{0.5}\text{Bi}_{0.5}\text{TiO}_3$ -5%BaTiO₃ (NBBT5), and $\text{Na}_{0.5}\text{Bi}_{0.5}\text{TiO}_3$ -8%K_{0.5}Bi_{0.5}TiO₃ (NKBT8) single crystals were grown by the top-seeded solution growth (TSSG) technique.²⁵ The samples were cut along the $\langle 001 \rangle$ face. Raman spectra at $\langle x|zz|y \rangle$ (VV) and $\langle x|zx|y \rangle$ (VH) configurations were carried out by a Jobin-Yvon LabRAM HR 800 UV spectrometer (Horiba International Corporation, Tokyo, Japan). Polarized spectra were recorded from 80 to 850 K by using a Linkam THMSE 600 heating/cooling stage (Linkam Scientific Instruments, Tadworth, U.K.). The He-Ne laser with the wavelength of 632.8 nm was taken as the exciting source. The near-normal incident ($\sim 10^\circ$) far-infrared (FIR) reflectance measurements were performed from 50 to 1000 cm^{-1} using a Bruker VERTEX 80 V Fourier-transform infrared spectrometer (Bruker Corporation, Billerica, MA).

The calculations are performed with density-functional theory (DFT) using the projector augmented wave (PAW) method, as implemented in the Vienna *ab initio* simulation package (VASP).²⁶ The exchange correlation potential is treated in Perdew–Burke–Ernzerhof (PBE) form of the generalized gradient approximation (GGA) with a kinetic-energy cutoff of 600 eV. A $7 \times 7 \times 7 \Gamma$ centered k -point grid is adopted in the self-consistent and phonon frequency calculations.²⁷ The convergence criterion for the electronic energy is 10^{-6} eV and the structures are relaxed until the Hellmann–Feynman forces on each atoms become less than 1 meV/Å.²⁸

The phonon modes and frequencies at the gamma point are carried out by the first-principles frozen-phonon method.²⁹ In order to simplify the calculations, the minimal 10-atom, 10-atom, and 20-atom cells with a specific 1:1 ordering of the A-site atoms (Na and Bi) are set to describe the unpolarized cubic phase, the polarized rhombohedral, and monoclinic phases, respectively.

III. Results and Discussion

The first-principle theoretical calculations provide information for atomic coordinates of NBT. The calculated lattice constants a_0 are 5.519 and 5.596 Å for cubic and rhombohedral phases, respectively, which are in good agreement with lattice parameter $a_0 = 5.484$ Å obtained by Rietveld refinement of synchrotron powder diffraction data with rhombohedral structure.¹⁹ Moreover, the calculated structural parameters of monoclinic phase a , b , c , and angle β are 9.755, 5.522, 5.629 Å, and 126.401° , which match well with the experimental data.^{15,19} The lattice parameters a , b , c , and angle β for monoclinic phase are reported as 9.526/9.520 Å, 5.483/5.480 Å, 5.508/5.511 Å, and $125.344^\circ/125.278^\circ$ by different authors.^{15,19} In case of cubic phase, Ti atom is in the center of oxygen octahedra and Na/Bi is in the center of oxygen cuboctahedra. The smallest Bi–Ti atomic distances in cubic, rhombohedral, and monoclinic structures are 3.38, 3.17, and 3.16 Å, respectively, which are consistent with the data of X-ray absorption fine structure measurements (3.22 Å).³⁰ That is, Bi atoms are displaced off from the high symmetry position in the cubic phase and form a shorter bond with the titanium atoms in the rhombohedral and monoclinic phases.

The depolarization and relaxor behavior of NBT-based solid solutions are caused by the existence of nonpolar or antiferroelectric phases. The zone-center optical phonon modes of cubic phase for NBT possess five irreducible representation: $A_{2u} + E_u + F_{2g} + 6F_{1u} + 2F_{2u}$, as shown in Fig. 1(a). A_{2u} and E_u are pure oxygen modes, and F_{2g} mode is the odd linear combination of two Ti atoms. There are five IR-active polar TO modes corresponding to atomic displacements of all atoms, and the rest one is the acoustic zero-frequency mode. Two F_{2u} modes are related to oxygen displacement patterns. Note that there are two unstable modes in F_{1u} at $187i \text{ cm}^{-1}$ and F_{2u} at $247i \text{ cm}^{-1}$. The former unstable mode F_{1u} is associated with triply degenerate and the atomic displacements are principally along the equivalent [001] direction, suggesting a transition trend from the cubic phase to the tetragonal phase.²² The latter unstable mode F_{2u} plays an important role in the rotation of the TiO₆ oxygen octahedra along the z -axis. Factor-group analysis predicts 18 IR and Raman-active modes for the rhombohedral phase of NBT in the absence of A-site disorder: $\Gamma_{R3c, \text{Raman}} = 9A_1 + 9E$. When A-site disorder is considered, five of the A_1 modes become silent. The modes A_1 and E are both infrared and Raman active. The A_1 symmetry is related to lattice displacements parallel to the c -axis of the unit cell, while the twofold-degenerate E mode is associated with phonons propagating perpendicular to the c -axis. Considering the splitting of each A_1 and E mode into the longitudinal optical and transverse optical components produced by IR and Raman activity, more modes are visible for the rhombohedral structure.^{22,23} We cannot see all of them because some modes become weak and overlapped. Relaxed atomic positions for the monoclinic structure are listed in Table I. The monoclinic phase with one effective Na/Bi atom would have $2A' + A''$. The Wyckoff positions $2a$ and $4b$ have fractional coordinates. The decompositions of the group theoretical irreducible representations (IRD) for the Wyckoff position at the zone-center Γ point are given.

Temperature dependence of polarized Raman spectra for NBT-based crystals is displayed in Figs. 1 and 2. The spectra were corrected for the Bose–Einstein temperature factor to

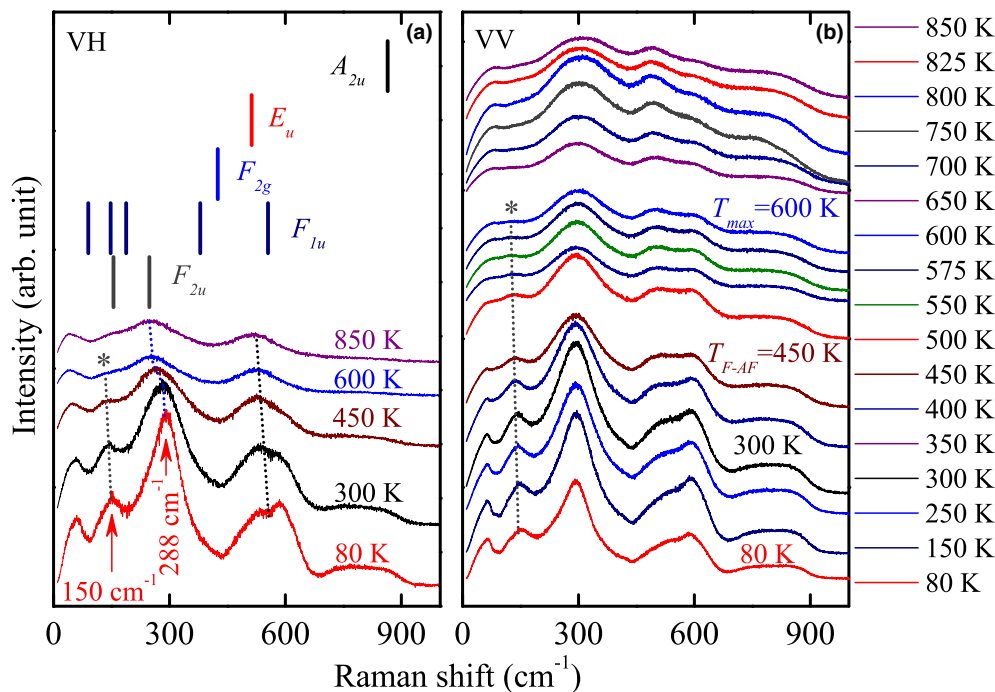


Fig. 1. (a) Calculated zone-center phonon mode frequencies of NBT in cubic structure. Phonon mode A_{2u} is at 864, E_u at 512, F_{2g} at 424, F_{1u} at 187i, 89, 147, 379, 554, and F_{2u} at 247i and 154 cm^{-1} , respectively. They are marked as compared with polarized Raman scattering. Raman spectra of the NKBT8 crystal in (a) $\langle x \text{ lz} x \rangle$ (VH) and (b) $\langle x \text{ lzz} \rangle$ (VV) scattering geometry, respectively. The asterisk and the dotted lines are marks of obvious broadening of the 150 cm^{-1} mode (Na–O vibration), which disappears above $T_{\text{max}} = 600$ K. $T_{\text{F-AF}}$ is the phase transition temperature from ferroelectric to antiferroelectric and T_{max} corresponds to the temperature of dielectric maximum. Note that each spectrum is shifted in intensity for clarity.

Table I. Relaxed Monoclinic Structure

| WP | Equivalent position | Relaxed position | IRD |
|----|-----------------------------|------------------|--------------|
| Na | 2a (0, 0.75, 0) | | $2A' + A''$ |
| Na | 2a (0.5, 0.75, 0.5) | | $2A' + A''$ |
| Bi | 2a (0, 0.25, 0.5) | | $2A' + A''$ |
| Bi | 2a (0.5, 0.25, 0) | | $2A' + A''$ |
| Ti | 2a (x, 0.25, z) | 0.277 (x) | $4A' + 2A''$ |
| | (0.5 + x, 0.25, 0.5 + z) | 0.238 (z) | |
| Ti | 2a (x, 0.75, z) | 0.268 (x) | $4A' + 2A''$ |
| | (0.5 + x, 0.75, z - 0.5) | 0.706 (z) | |
| O1 | 2a (x, 0.25, z) | 0.035 (x) | $4A' + 2A''$ |
| | (0.5 + x, 0.25, 0.5 + z) | 0.238 (z) | |
| O1 | 2a (x, 0.75, z) | 0.034 (x) | $4A' + 2A''$ |
| | (0.5 + x, 0.75, z - 0.5) | 0.464 (z) | |
| O2 | 4b (x, y, z) | 0.292 (x) | $6A' + 6A''$ |
| | (0.5 + x, y, 0.5 + z) | 0.485 (y) | |
| | (x, 0.5 - y, z) | -0.049 (z) | |
| | (0.5 + x, 0.5 - y, 0.5 + z) | | |
| O3 | 4b (x, y, z) | 0.289 (x) | $6A' + 6A''$ |
| | (0.5 + x, y, 0.5 + z) | 0.485 (y) | |
| | (x, 0.5 - y, z) | 0.464 (z) | |
| | (0.5 + x, 0.5 - y, 0.5 + z) | | |

WP stands for Wyckoff positions. IRD is decomposition of the group theoretical irreducible representation at the Γ point. Calculated frequencies of 36 A' modes for the monoclinic structure of NBT are at 55i, 0.9i, 0.7i, 74, 101, 104, 119, 132, 144, 152, 189, 193, 200, 250, 262, 273, 289, 306, 317, 333, 353, 362, 397, 405, 447, 449, 457, 489, 539, 583, 597, 629, 633, 790, 834, 868 cm^{-1} , and 24 A'' modes are at 151i, 85i, 60i, 53i, 0.6, 49, 120, 153, 169, 176, 223, 225, 249, 253, 261, 290, 333, 341, 395, 400, 514, 533, 635, 644 cm^{-1} .

eliminate the contribution of the Bose–Einstein population factor from the measured Raman intensity. The reduced Raman intensity is written as $R(\nu) = I(\nu)/[n(\nu) + 1]$, where $I(\nu)$ is the measured Raman intensity and $n(\nu) = (e^{h\nu/kT} - 1)^{-1}$

is the Bose–Einstein factor. The spectra are in good agreement with those from reported NBT-based perovskites.³¹ Raman bands are relatively broad, mainly due to the disorder on the A-site. The modes below 150 cm^{-1} are related to the vibrations of the A-site, including Bi, Na, K, and Ba. The existence of such obvious modes in the frequency range indicates possible cation ordering at the A-site. The atomic mass of bismuth m_{Bi} is 208.98. Compared with the heavy bismuth cation, sodium ($m_{\text{Na}} = 22.99$) and potassium ($m_{\text{K}} = 39.10$) have similar atomic mass, which means that a mass effect can be negligible for most of the phonon modes, except for those involving these cations. Note that the ionic radii of K^+ and Ba^{2+} ($r_{\text{K}^+} = 1.33 \text{ \AA}$, $r_{\text{Ba}^{2+}} = 1.35 \text{ \AA}$) are larger than that of Na^+ ($r_{\text{Na}^+} = 1.02 \text{ \AA}$). The increase in the ionic radii results in a distortion of the structure, which leads to a high-frequency shift.¹² Considering the cation mass on the A-site, the modes at 150 and 120 cm^{-1} correspond to Na–O and K–O vibrations, respectively. Their appearance below T_{max} indicates the existence of nanosized $(\text{Na}_{1-x}\text{K}_x)^+\text{TiO}_3$ clusters, otherwise the phonon lifetime would have been too short to result in a defined Raman band.³² The modes in the frequency of 150–450 cm^{-1} are related to Ti–O vibrations. The remarkable redshift of 280 cm^{-1} mode in the VH geometry is seen with increasing temperature, as shown in Fig. 3. It is assigned as an A_1 mode, representing the strength of the Ti–O bond. Bands between 450 and 700 cm^{-1} are related to TiO_6 vibrations, which is the breathing and stretching modes of the oxygen octahedra. The high-frequency bands from 700 to 900 cm^{-1} are regarded as overlapping between the $A_1(\text{LO})$ and $E(\text{LO})$ modes so far, by assuming the fact that pure NBT is rhombohedral phase at room temperature.

The present Raman spectra and first-principle calculation reveal the coexistence of monoclinic and rhombohedral phases for NBT at room temperature, which agrees well with recent evidences detected by X-ray powder diffraction,^{14,15} neutron powder diffraction,¹⁹ and transmission electron microscopy.²⁴ The observed Raman-active mode at 860 cm^{-1} is assigned as A' mode (868 cm^{-1} from calculation) in mono-

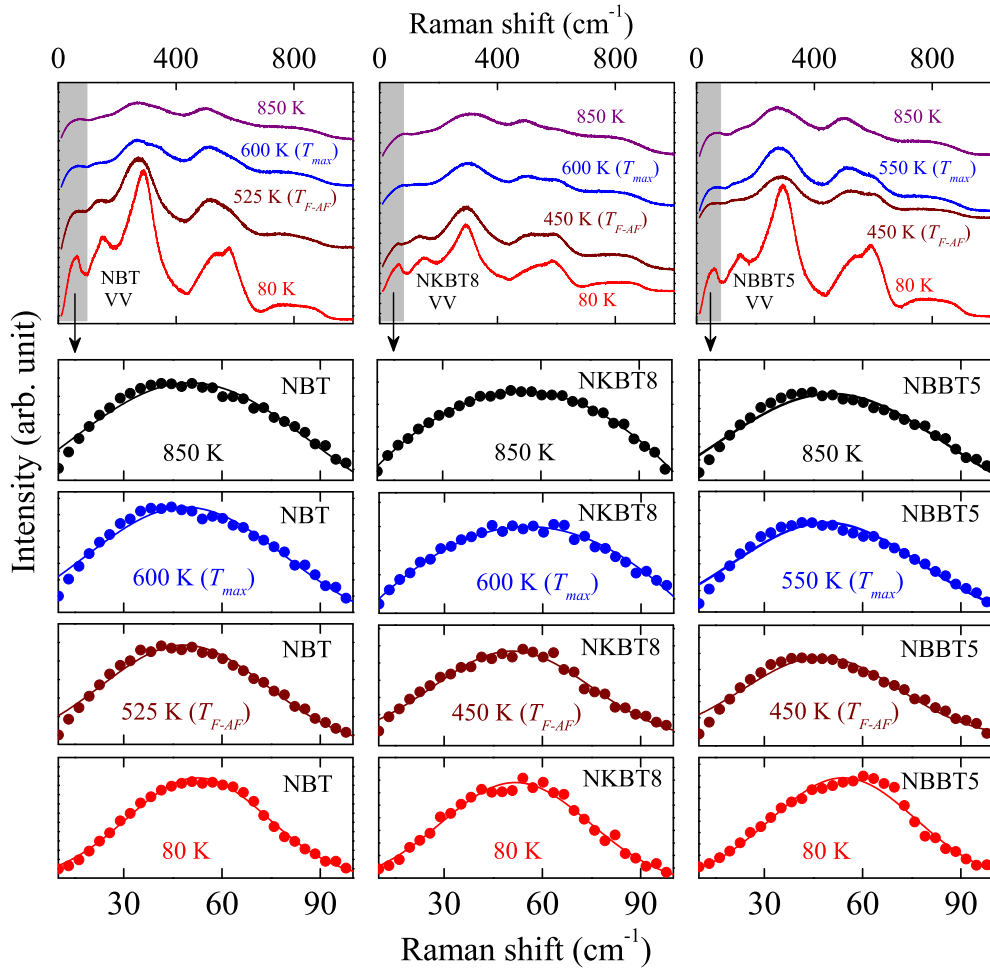


Fig. 2. Polarized Raman spectra of NBT, NKBT8, and NBBT5 crystals at selected temperatures. The overlapped bands between 10 and 100 cm^{-1} have been deconvoluted after baseline correction.

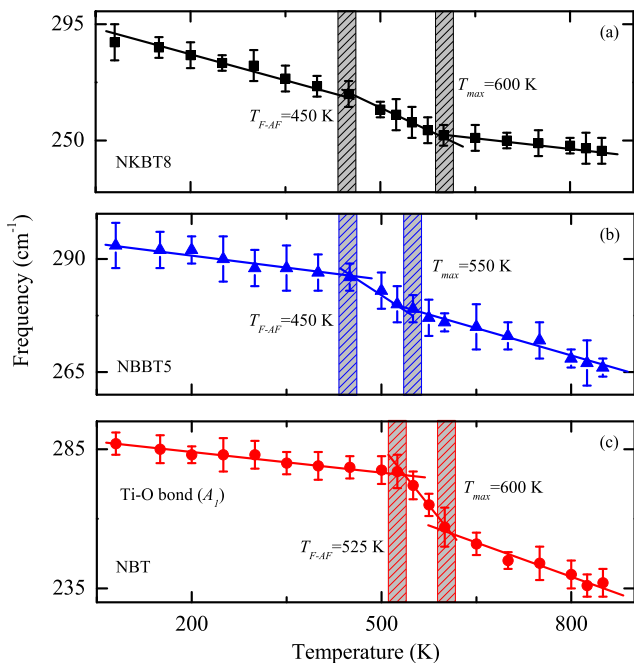


Fig. 3. Temperature dependence of phonon mode frequency for NKBT8, NBBT5, and NBT crystals. Note that the distinct variation trends appear across the ferroelectric to antiferroelectric phase transition temperature T_{F-AF} and T_{max} corresponding to the temperature of dielectric maximum, respectively.

clinic phase, rather than previously assumed A_1 mode in rhombohedral phase (820 or 830 cm^{-1} from the calculation).^{22,23} Therefore, the high-frequency bands are related to overlap among the $A_1(\text{LO})$, $E(\text{LO})$, and A' modes contributed from rhombohedral and monoclinic phases. Moreover, the observed Raman-active mode at 385 cm^{-1} is A'' in the monoclinic phase instead of A_1 in the rhombohedral structure. As listed in Table II, a phonon mode at 385 cm^{-1} is assigned as A'' at 395 cm^{-1} of monoclinic phase, instead of previously assumed A_1 at 402 or 398 cm^{-1} . A phonon mode appears at 54 cm^{-1} , which is assigned as A'' from monoclinic structure. Such low-frequency vibrational mode has not been assigned so far in NBT, mainly due to the existence of rhombohedral phase instead of coexistence of monoclinic and rhombohedral phases before. For example, the lowest calculated phonon frequencies for rhombohedral structure is at 108 cm^{-1} as E mode, similar to that reported from others (109 or 116 cm^{-1}),^{22,23} which cannot explain the vibration modes below 100 cm^{-1} . The presence of such low mode below 100 cm^{-1} was assumed as Bi-O bond, because measured and calculated phonon frequencies in $\alpha\text{-Bi}_2\text{O}_3$ revealed the existence of A_g and B_g modes at 52 and 58 cm^{-1} or 40 and 57 cm^{-1} for the experiment and calculation, respectively.³² Note that the frequencies of A_g and B_g modes are grouped in pairs.

Coexistence of ferroelectric monoclinic phase and other ferroelectric phases including rhombohedral or tetragonal structure is reported in other perovskite-type relaxor systems. For instance, in the MPB region for PZT or PMN-PT system, a monoclinic phase was observed as a bridging phase,

Table II. Calculated Frequencies for the Rhombohedral and Monoclinic Structures of NBT

| Frequency Exp./Cal. | This work Phonon modes | Ref. [22] Cal. | Ref. [23] Exp./Cal. |
|------------------------|---------------------------|-------------------|------------------------|
| 54/49 | A'' | — | — |
| 141/133 | A_1 | 137 | 141/134 |
| 213/211 | A_1 | 234 | 235/233 |
| 283/278 | A_1 | 280 | 274/276 |
| 385/395 | A'_1 | 402 (A_1) | -/398 (A_1) |
| 501/510 | E | 547 | 527/549 |
| 585/583 | A_1 | 575 | 573/575 |
| 595/597 | E | 591 | -/594 |
| 763/790 | A'_1 | — | 750/737 (A_1) |
| 860/868 | A'_1 | 820 (A_1) | 869/830 (A_1) |

The phonon mode frequencies of the NBT single crystal are extracted from the Gaussian curve fitting [Fig. 4(d)] at 300 K. The experimental and theoretical data from the NBT crystals have been taken from Refs. [22] and [23] for comparison. Note that the unit is cm^{-1} .

which mediates the structural transition from rhombohedral to tetragonal phase.³³ Since the extraordinary piezoelectric properties and monoclinic phase were found in the MPB region, a long debate on the relationship between the monoclinic phase and the giant piezoelectric response was ignited. However, NBT has rather moderate piezoelectric coefficients. The present work reports a coexistence of monoclinic and rhombohedral structures in pure NBT, showing no close relationship between monoclinic phase and large piezoelectricity. The high piezoelectric response in NBT-based systems is associated with the mechanism of polarization rotation. It is similar to that in lead-based relaxors, with the highest piezoelectricity appearing along the $[001]_{\text{cub}}$ -poling direction rather than along the $[111]_{\text{cub}}$ -polar directions of the rhombohedral phase. According to the polarization rotation theory, ferro-

electric-ferroelectric instability is related to the formation of a bridging monoclinic phase, providing continuous low energy pathways for polarization vector to rotate under application of external electric field.³⁴

A weakening of the bonding between the A-site cation and oxygen leads to the softening of A-site modes with increasing temperature. The anomaly at 525 K ($T_{\text{F-AF}}$) is associated with the loss of orbital hybridization between the $6s^2$ orbitals of the Bi^{3+} and the oxygen p orbitals due to the presence of a lone pair in Bi^{3+} .³¹ Note that high Curie temperature of lead titanate (PbTiO_3)-based solid solutions is due to the hybridization of the A-site lone pairs with oxygen.³⁵ The first-principle study of PbTiO_3 indicates that the rotation of TiO_6 octahedron and the ferroelectric displacement are dominated by the Pb–O and Ti–O covalent interactions. Moreover, ferroelectric or antiferrodistortive phase transitions are governed by the balance between the strength of the Pb–O and Ti–O covalent interactions.³⁶ The hybridization of Pb 6s valence electrons with O 2p states as well as the displacements of the Pb^{2+} ions is regarded as the main factors for the enhanced ferroelectric properties.³⁷ Octahedral tilting in perovskites can be controlled by variations of covalent bonding through the mixing of occupied and unoccupied orbitals driven by the distortion. A hybridization and shift in electron density from oxygen to Ti^{4+} can be caused by the empty d -shell of the central atom. Similar process was found in oxides containing a d^0 transition metal (Ti^{4+} , Nb^{5+} , W^{6+} , etc.) and a lone-pair cation.³⁸

Three main IR modes are observed near 100, 320, and 620 cm^{-1} . Compared with IR spectra in Fig. 4, the Raman modes near 150 and 530 cm^{-1} are regarded as the IR modes activated due to the breaking of the inversion.³⁹ The broad Raman hump near 800 cm^{-1} corresponds to the weak IR mode. This is in good agreement with calculated frequency of A_1 mode at 793 cm^{-1} for NBT. The disagreement between the theoretical and experimental data is due to the absence

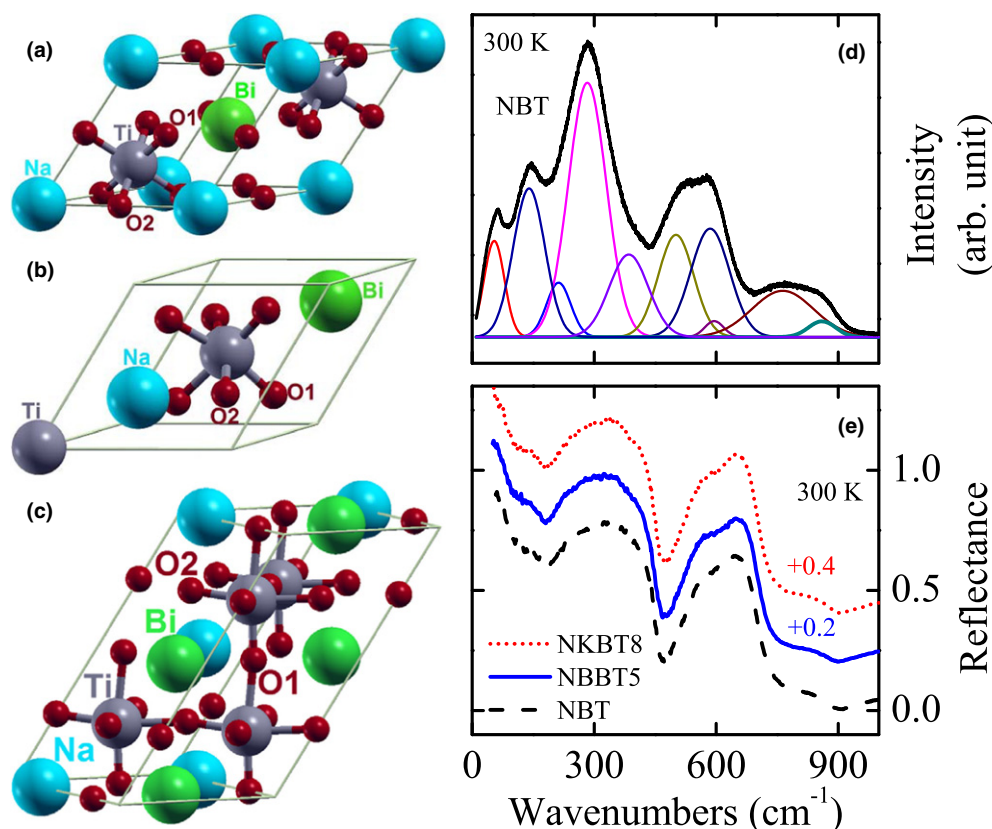


Fig. 4. The unit cells of (a) cubic, (b) rhombohedral, and (c) monoclinic phases of NBT. (d) Deconvolution of the Raman spectra at 300 K. (e) Infrared reflectance spectra of NBT, NBBT5, and NKBT8 crystals at room temperature.

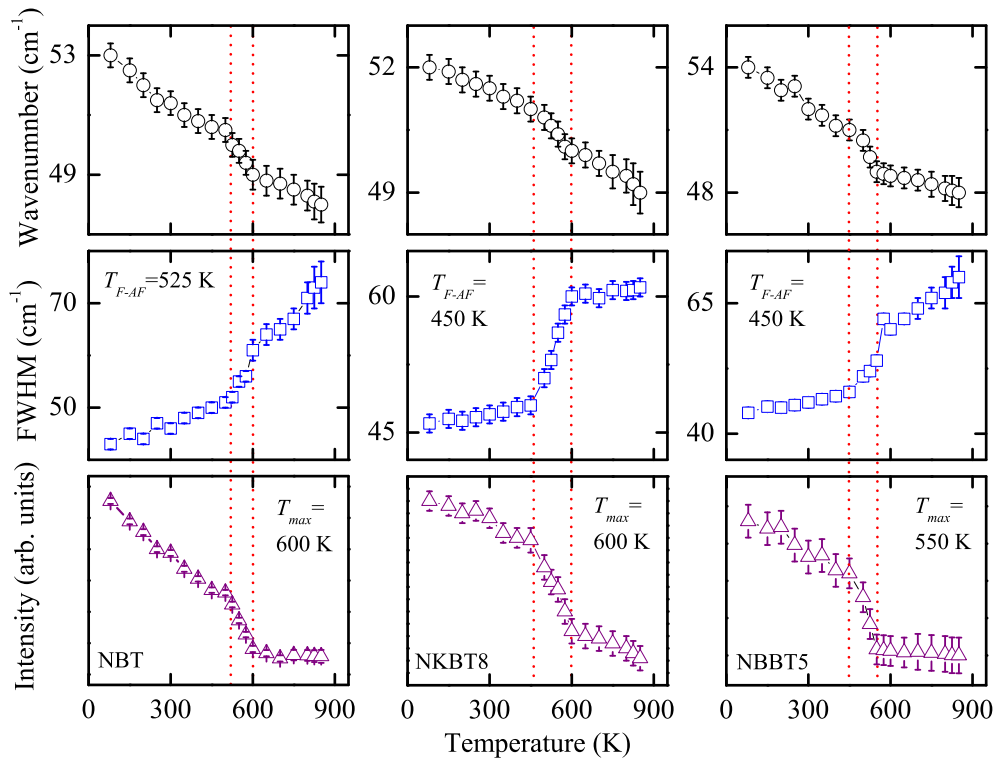


Fig. 5. Temperature dependence of the peak position, intensity, and full width at half maximum (FWHM) on the A'' mode around 49 cm^{-1} for NBT, NKBT8, and NBBT5 crystals, respectively.

of A-site disorder in the theoretical model and temperature difference. The temperature evolution of the peak position, full width at half maximum (FWHM), and intensity for the A'' mode at 49 cm^{-1} are associated with phase transitions. In the absence of phase transitions, one would expect a phonon mode softening and a steady increase in FWHM with increasing temperature. It demonstrates a smooth decrease in the unit-cell anisotropy with increasing temperature. For NBT-based systems, the phase transitions occur mainly in one crystallographic direction.³¹ With increasing temperature, a more disordered lattice is obtained. This is mediated by a weakening of the Bi–O hybrid orbitals, which leads to an enhanced polarizability of the unit cell. Two frequency deviations from linearity are observed at 525 and 600 K for NBT, 425 and 550 K for NBBT5, and 450 and 600 K for NKBT8, as shown in Figs. 3 and 5. They are associated with the ferroelectric–antiferroelectric phase transitions temperature T_{F-AF} and T_{max} corresponding to the temperature of dielectric maximum ϵ_m . For NBT and NBBT5, our results are in good agreement with phase diagram of NBBT by anelastic and dielectric measurements.^{40,41} The ferroelectric–antiferroelectric phase transition temperatures T_{F-AF} were reported as 523 K for NBT and 450/473 K for NBBT5, while T_{max} were 603 K for NBT and 550/543 K for NBBT5.^{40,41} For NKBT8, it agrees well with dielectric constant measurement, which shows that the parameter T_{max} is located between 589 and 591 K according to different orientations ($\langle 001 \rangle$, $\langle 110 \rangle$, $\langle 111 \rangle$) of NKBT8.²⁵ It indicates that the dielectric anisotropy is rather weak. The red shifts of frequency with increasing temperature for A'' mode and Ti–O bond suggest that the particular phonons are directly involved in the phase transitions.

IV. Conclusions

As a result of polarized Raman spectra and first-principle calculation, the assignment of the bands to certain vibrational modes is carried out by consideration of both rhombohedral and monoclinic phases. It is found that three Raman-active phonon modes at 395 , 790 , and 868 cm^{-1} are A'' , A' , and A'

modes of monoclinic phase instead of A_1 modes from rhombohedral phase assumed so far. Furthermore, a low-frequency phonon mode at 49 cm^{-1} is assigned as A'' and its temperature dependence is provided. Structural changes in NBT-based solid solutions are revealed by polarized Raman and IR spectra. Group-theory predicts two unstable modes F_{1u} at $187i\text{ cm}^{-1}$ and F_{2u} at $247i\text{ cm}^{-1}$ in cubic structure, which indicate a phase transition trend from cubic structure to tetragonal structure. Two frequency deviations from linearity are observed at 525 and 600 K for NBT crystal, 425 and 550 K for NBBT5 crystal, and 450 and 600 K for NKBT8 crystal, respectively. The present results improve the knowledge of the coexistence of ferroelectric phases in pure NBT and ferroelectric phase transitions in NBT-based systems.

Acknowledgments

One of the authors (J. J. Zhu) is grateful to Prof. Chungang Duan and Dr. Wenyi Tong for the technical supports. This work was financially supported by Major State Basic Research Development Program of China (grant nos. 2011CB922200 and 2013CB922300), Natural Science Foundation of China (grant nos. 11374097, 61376129, and 61504156), Projects of Science and Technology Commission of Shanghai Municipality (grant nos. 15JC1401600, 14XD1401500, 13JC1402100, 13JC1404200, and 15YF1413900), the Program for Professor of Special Appointment (Eastern Scholar) at Shanghai Institutions of Higher Learning, and Project funded by China Postdoctoral Science Foundation (grant no. 2014M560357).

References

- R. E. Cohen, "Origin of Ferroelectricity in Perovskite Oxides," *Nature*, **358** [6382] 136–8 (1992).
- H. Fu and R. E. Cohen, "Polarization Rotation Mechanism for Ultrahigh Electromechanical Response in Single-Crystal Piezoelectrics," *Nature*, **403** [6767] 281–3 (2000).
- P. G. Fernandez, J. A. Aramburu, M. T. Barriuso, and M. Moreno, "Key Role of Covalent Bonding in Octahedral Tilting in Perovskites," *J. Phys. Chem. Lett.*, **1** [3] 647–51 (2010).
- J. J. Zhu, J. Z. Zhang, G. S. Xu, X. L. Zhang, Z. G. Hu, and J. H. Chu, "Electronic Transitions and Dielectric Functions of Relaxor Ferroelectric $\text{Pb}(\text{In}_{1/2}\text{Nb}_{1/2})\text{O}_3\text{-Pb}(\text{Mg}_{1/3}\text{Nb}_{2/3})\text{O}_3\text{-PbTiO}_3$ Single Crystals: Temperature Dependent Spectroscopic Study," *Appl. Phys. Lett.*, **104** [13] 132903, 5pp (2014).

- ⁵V. V. Shvartsman and D. C. Lupascu, "Lead-Free Relaxor Ferroelectrics," *J. Am. Ceram. Soc.*, **95** [1] 1–26 (2012).
- ⁶B. W. Eerd, D. Damjanovic, N. Klein, N. Setter, and J. Trodahl, "Structural Complexity of $(\text{Na}_{0.5}\text{Bi}_{0.5})\text{TiO}_3\text{-BaTiO}_3$ as Revealed by Raman Spectroscopy," *Phys. Rev. B*, **82** [10] 104112, 7pp (2010).
- ⁷D. Kirsever and H. Yilmaz, "Electrical Properties of Lead-Free $\text{Na}_{1/2}\text{Bi}_{1/2}\text{TiO}_3$ Relaxor Ferroelectric Ceramics Doped With Hafnium or Zirconium," *J. Am. Ceram. Soc.*, **98** [6] 1858–64 (2015).
- ⁸R. Ramesh and N. A. Spaldin, "Multiferroics: Progress and Prospects in Thin Films," *Nature Mater.*, **6** [1] 21–9 (2007).
- ⁹D. S. Keeble, E. R. Barney, D. A. Keen, M. G. Tucker, J. Kreisel, and P. A. Thomas, "Bifurcated Polarization Rotation in Bismuth-Based Piezoelectrics," *Adv. Funct. Mater.*, **23** [2] 185–90 (2013).
- ¹⁰W. W. Ge, H. Cao, C. DeVreugd, J. F. Li, D. Viehland, et al., "Influence of BaTiO_3 Content on the Structure and Properties of $\text{Na}_{0.5}\text{Bi}_{0.5}\text{TiO}_3$ Crystals," *J. Am. Ceram. Soc.*, **94** [9] 3084–7 (2011).
- ¹¹H. B. Zhang, S. L. Jiang, and K. Kajiyoshi, "Pyroelectric and Dielectric Properties of Mn Modified $0.82\text{Bi}_{0.5}\text{Na}_{0.5}\text{TiO}_3\text{-}0.18\text{Bi}_{0.5}\text{K}_{0.5}\text{TiO}_3$ Lead-Free Thick Films," *J. Am. Ceram. Soc.*, **92** [9] 2147–50 (2009).
- ¹²J. Kreisel, A. M. Glazer, G. Jones, P. A. Thomas, L. Abello, and G. Lucazeau, "An X-ray Diffraction and Raman Spectroscopy Investigation of A-Site Substituted Perovskite Compounds: The $(\text{Na}_{1-x}\text{K}_x)_0.5\text{Bi}_{0.5}\text{TiO}_3$ ($0 \leq x \leq 1$) Solid Solution," *J. Phys.: Condens. Matter*, **12** [14] 3267, 14pp (2000).
- ¹³C. Ma, H. Guo, S. P. Bechman, and X. Tan, "Creation and Destruction of Morphotropic Phase Boundaries Through Electrical Poling: A Case Study of Lead-Free $(\text{Bi}_{1/2}\text{Na}_{1/2})\text{TiO}_3\text{-BaTiO}_3$ Piezoelectrics," *Phys. Rev. Lett.*, **109** [10] 107602, 5pp (2012).
- ¹⁴S. Gorfman and P. A. Thomas, "Evidence for a Non-Rhombohedral Average Structure in the Lead-Free Piezoelectric Material $\text{Na}_{0.5}\text{Bi}_{0.5}\text{TiO}_3$," *J. Appl. Crystallogr.*, **43** [6] 1409–14 (2010).
- ¹⁵E. Aksel, J. S. Forrester, J. L. Jones, P. A. Thomas, K. Page, and M. R. Suchomel, "Monoclinic Crystal Structure of Polycrystalline $\text{Na}_{0.5}\text{Bi}_{0.5}\text{TiO}_3$," *Appl. Phys. Lett.*, **98** [15] 152901, 3pp (2011).
- ¹⁶E. Aksel, J. S. Forrester, B. Kowalski, M. Deluca, D. Damjanovic, and J. L. Jones, "Structure and Properties of Fe-Modified $\text{Na}_{0.5}\text{Bi}_{0.5}\text{TiO}_3$ at Ambient and Elevated Temperature," *Phys. Rev. B*, **85** [2] 024121, 11pp (2012).
- ¹⁷B. N. Rao, M. Avdeev, B. Kennedy, and R. Ranjan, "Phase Boundary at $x = 0.03$ and its Anomalous Influence on the Structure and Properties in the Lead-Free Piezoelectric $(1-x)\text{Na}_{0.5}\text{Bi}_{0.5}\text{TiO}_3\text{-}x\text{BaTiO}_3$," *Phys. Rev. B*, **92** [21] 214107, 11pp (2015).
- ¹⁸B. N. Rao, A. N. Fitch, and R. Ranjan, "Ferroelectric-Ferroelectric Phase Coexistence in $\text{Na}_{0.5}\text{Bi}_{0.5}\text{TiO}_3$," *Phys. Rev. B*, **87** [6] 060102(R), 5pp (2013).
- ¹⁹B. N. Rao, R. Datta, S. S. Chandrashekar, D. K. Mishra, V. Sathe, et al., "Local Structural Disorder and its Influence on the Average Global Structure and Polar Properties in $\text{Na}_{0.5}\text{Bi}_{0.5}\text{TiO}_3$," *Phys. Rev. B*, **88** [22] 224103, 15pp (2013).
- ²⁰J. J. Zhu, K. Jiang, G. S. Xu, Z. G. Hu, Y. W. Li, et al., "Temperature-Dependent Raman Scattering and Multiple Phase Coexistence in Relaxor Ferroelectric $\text{Pb}(\text{In}_{1/2}\text{Nb}_{1/2})\text{O}_3\text{-Pb}(\text{Mg}_{1/3}\text{Nb}_{2/3})\text{O}_3\text{-PbTiO}_3$ Single Crystals," *J. Appl. Phys.*, **114** [15] 153508, 10pp (2013).
- ²¹J. J. Zhu, W. W. Li, G. S. Xu, K. Jiang, Z. G. Hu, and J. H. Chu, "A Phenomenological Model of Electronic Band Structure in Ferroelectric $\text{Pb}(\text{In}_{1/2}\text{Nb}_{1/2})\text{O}_3\text{-Pb}(\text{Mg}_{1/3}\text{Nb}_{2/3})\text{O}_3\text{-PbTiO}_3$ Single Crystals Around Morphotropic Phase Boundary Determined by Temperature-Dependent Transmittance Spectra," *Acta Mater.*, **59** [17] 6684–90 (2011).
- ²²H. F. Lu, S. Y. Wang, and X. S. Wang, "The Electronic Properties and Lattice Dynamics of $(\text{Na}_{0.5}\text{Bi}_{0.5})\text{TiO}_3$: From Cubic to Tetragonal and Rhombohedral Phases," *J. Appl. Phys.*, **115** [12] 124107, 7pp (2014).
- ²³M. K. Niranjana, T. Karthik, S. Asthana, J. Pan, and U. V. Waghmare, "Theoretical and Experimental Investigation of Raman Modes, Ferroelectric and Dielectric Properties of Relaxor $\text{Na}_{0.5}\text{Bi}_{0.5}\text{TiO}_3$," *J. Appl. Phys.*, **113** [19] 194106, 7pp (2013).
- ²⁴I. Levin and I. M. Reaney, "Nano- and Mesoscale Structure of $\text{Na}_{1/2}\text{Bi}_{1/2}\text{TiO}_3$: A TEM Perspective," *Adv. Funct. Mater.*, **22** [16] 3445–52 (2012).
- ²⁵R. B. Sun, X. Y. Zhao, Q. H. Zhang, B. J. Fang, H. W. Zhang, et al., "Growth and Orientation Dependence of Electrical Properties of 0.92 $\text{Na}_{0.5}\text{Bi}_{0.5}\text{TiO}_3\text{-}0.08\text{K}_{0.5}\text{Bi}_{0.5}\text{TiO}_3$ Lead-Free Piezoelectric Single Crystal," *J. Appl. Phys.*, **109** [12] 124113, 8pp (2011).
- ²⁶G. Kresse and J. Furthmüller, "Efficient Iterative Schemes for *ab Initio* Total-Energy Calculations Using a Plane-Wave Basis Set," *Phys. Rev. B*, **54** [16] 11169–86 (1996).
- ²⁷J. P. Perdew, K. Burke, and M. Ernzerhof, "Generalized Gradient Approximation Made Simple," *Phys. Rev. Lett.*, **77** [18] 3865–8 (1996).
- ²⁸P. E. Blöchl, O. Jepsen, and O. K. Andersen, "Improved Tetrahedron Method for Brillouin-Zone Integrations," *Phys. Rev. B*, **49** [23] 16223–33 (1994).
- ²⁹W. Y. Tong, H. C. Ding, Y. C. Gao, S. J. Gong, X. G. Wan, and C. G. Duan, "Spin-Dependent Optical Response of Multiferroic EuO: First-Principles DFT Calculations," *Phys. Rev. B*, **89** [6] 064404, 8pp (2014).
- ³⁰V. A. Shuvaeva, D. Zekria, A. M. Glazer, Q. Jiang, S. M. Weber, et al., "Local Structure of the Lead-Free Relaxor Ferroelectric $(\text{K}_x\text{Na}_{1-x})_{0.5}\text{Bi}_{0.5}\text{TiO}_3$," *Phys. Rev. B*, **71** [17] 174114, 8pp (2005).
- ³¹D. Schutz, M. Deluca, W. Krauss, A. Feteira, T. Jackson, and K. Reichmann, "Lone-Pair-Induced Covalency as the Cause of Temperature- and Field-Induced Instabilities in Bismuth Sodium Titanate," *Adv. Funct. Mater.*, **22** [11] 2285–94 (2012).
- ³²V. N. Denisov, A. N. Ivlev, A. S. Lipin, B. N. Mavrin, and V. G. Orlov, "Raman Spectra and Lattice Dynamics of Single-Crystal $\alpha\text{-Bi}_2\text{O}_3$," *J. Phys.: Condens. Matter*, **9** [23] 4967–78 (1997).
- ³³R. A. Cowley, S. N. Gvasaliya, S. G. Lushnikov, B. Roessli, and G. M. Rotaru, "Relaxing With Relaxors: A Review of Relaxor Ferroelectrics," *Adv. Phys.*, **60** [2] 229–327 (2011).
- ³⁴D. Vanderbilt and M. H. Cohen, "Monoclinic and Triclinic Phases in Higher-Order Devonshire Theory," *Phys. Rev. B*, **63** [9] 094108, 9pp (2001).
- ³⁵G. Shirane, R. Pepinsky, and B. C. Frazer, "X-ray and Neutron Diffraction Study of Ferroelectric PbTiO_2 ," *Acta Crystallogr.*, **9** [2] 131–40 (1956).
- ³⁶H. Kawanishi, K. Ishizumi, I. Takahashi, H. Terauchi, and Y. Hayafuji, "Comparative First-Principles Study of ATiO_3 Perovskite Oxides (A=Ba, Sr, and Pb)," *Jpn. J. Appl. Phys.*, **46** [3A] 1067–70 (2007).
- ³⁷W. L. Warren, J. Robertson, D. Dimos, B. A. Tuttle, G. E. Pike, and D. A. Payne, "Pb Displacements in $\text{Pb}(\text{Zr,Ti})\text{O}_3$ Perovskites," *Phys. Rev. B*, **53** [6] 3080–7 (1996).
- ³⁸P. S. Halasyamani, "Asymmetric Cation Coordination in Oxide Materials: Influence of Lone-Pair Cations on the Intra-Octahedral Distortion in d^0 Transition Metals," *Chem. Mater.*, **16** [19] 3586–92 (2004).
- ³⁹J. Petzelt, S. Kamba, J. Fabry, D. Noujni, V. Porokhonskyy, et al., "Infrared, Raman and High-Frequency Dielectric Spectroscopy and the Phase Transitions in $(\text{Na}_{1/2}\text{Bi}_{1/2})\text{TiO}_3$," *J. Phys.: Condens. Matter*, **16** [15] 2719–32 (2004).
- ⁴⁰W. W. Ge, C. T. Luo, Q. H. Zhang, Y. Ren, J. F. Li, et al., "Evolution of Structure in $\text{Na}_{0.5}\text{Bi}_{0.5}\text{TiO}_3$ Single Crystals With BaTiO_3 ," *Appl. Phys. Lett.*, **105** [16] 162913, 5pp (2014).
- ⁴¹F. Cordero, F. Craciun, F. Trequattrini, E. Mercadelli, and C. Galassi, "Phase Transitions and Phase Diagram of the Ferroelectric Perovskite $(1-x)\text{Na}_{0.5}\text{Bi}_{0.5}\text{TiO}_3\text{-}x\text{BaTiO}_3$ by Anelastic and Dielectric Measurements," *Phys. Rev. B*, **81** [14] 144124, 10pp (2010). □